ACS APPLIED ENERGY MATERIALS

www.acsaem.org Article

Toward Moisture-Stable and Dendrite-Free Garnet-Type Solid-State Electrolytes

Sathish Rajendran, Naresh Kumar Thangavel, Kiran Mahankali, and Leela Mohana Reddy Arava*

Cite This: *ACS Appl. Energy Mater.* 2020, 3, 6775−6784 Read Online

ABSTRACT: All-solid-state batteries using garnet-type solid-state electrolytes (SSEs) are promising candidates for safe, high energy density batteries due to their wide electrochemical stability window, high lithium-ion conductivity at room temperature, and the use of a lithium metal anode. However, garnet-type SSEs exhibit formidable challenges, including their instability in a moisture-containing atmosphere, high interfacial resistance, and the formation of lithium dendrites. Though several strategies have been deployed to alleviate the issues related to garnet-type SSEs against metallic lithium, most of the approaches fail to solve all the challenges. Herein, we demonstrate a surface modification strategy of the $Li_{6.5}La_3Zr_{1.5}Ta_{0.5}O_{12}$ (LLZT) garnet electrolyte by two-dimensional hexagonal boron nitride (h-BN) nanosheets to solve the interfacial issues. Detailed spectroscopic evidence elucidates that the h-BN interlayer effectively protects the LLZT from moisture-induced chemical degradation and suppresses the formation of adverse carbonate species for over 120 h in an open atmosphere. The h-BN-coated garnet SSE interface has shown a nearly 10-fold reduction in interfacial resistance value compared to the uncoated one and it exhibits stable lithium plating/stripping behavior for over 1400 cycles at 0.2 mA cm^{-2}. Advanced in situ Raman analysis reveals that the h-BN interlayers remain stable during cycling and inhibit the structural transformation of LLZT at the interface.

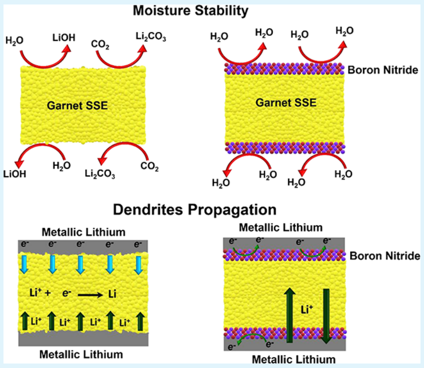

KEYWORDS: *solid-state electrolyte, garnet electrolyte, h-BN, moisture stability, dendrite suppression, in-situ Raman, lithium metal anode*

■ INTRODUCTION

Lithium-ion batteries (LIBs) are becoming increasingly ubiquitous energy storage systems to power most portable electronic devices due to their high energy densities and long cycle life.[1,2] However, with extending applications of LIBs into electrifying transport and grid storage, an increase in their performance is essential to meet today's requirements.[3] Besides, the safety of LIBs remains a major concern due to the use of highly flammable organic liquid electrolytes, which have a low flash point and carry the risk of leakage, fire, and explosion.[4] All-solid-state batteries (ASSBs) provide potential solutions to the major drawbacks of LIBs.[5,6] ASSBs with suitable solid-state electrolytes (SSEs) enable the use of a metallic lithium (Li) anode, which exhibits a highest specific capacity of 3861 mAh g^{-1} and lowest reduction potential (−3.05 V) to achieve high energy density and safer batteries that meet the growing energy demands.[7] The main SSEs include LiSICON,[8] garnet-type,[9,10] sulfide-based glass/ceramic,[11] perovskite,[12] antiperovskite,[13] NASICON-type materials,[14,15] etc. Among these, garnet-type SSEs exhibit exceptional properties, including high chemical stability against metallic Li,[16] high Li-ion conductivity (∼10^{-3} S cm^{-1}),[17,18] and wide electrochemical stability window (∼6 V vs Li/Li$^+$) that enables the use of high voltage cathodes.[16,19]

Despite the manifold advantages offered by garnet-type SSEs, a few challenges, such as high interfacial resistance and dendrite formation even at lower current densities hinder their targeted applications.[20,21] The high interfacial resistance originates from the poor wettability of the garnet SSE with metallic Li at the interface.[19,22,23] This can be attributed to the unstable nature of the garnet surface against a moisture-containing environment where proton-lithium (H$^+$/Li$^+$) exchange takes place. This interchange reaction leads to the formation of insulating lithium carbonate (Li_2CO_3) through intermediates (as shown in eqs 1 and 2), which blocks the Li-ion transport across the interface.[24−26] Although efforts were made to remove the lithium carbonate layer from the garnet surface,[27,28] there are no studies that prevent the formation of lithium carbonate on the surface of the solid electrolyte altogether.

$$Li_{6.4}La_3Zr_{1.4}Ta_{0.6}O_{12} + xH_2O \rightarrow Li_{6.4-x}H_xLa_3Zr_{1.4}Ta_{0.6}O_{12} + xLiOH \quad (1)$$

$$2LiOH + CO_2 \rightarrow Li_2CO_3 + H_2O \quad (2)$$

Received: April 21, 2020
Accepted: June 3, 2020
Published: June 3, 2020

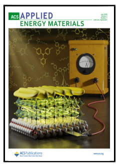

https://dx.doi.org/10.1021/acsaem.0c00905
ACS Appl. Energy Mater. 2020, 3, 6775−6784

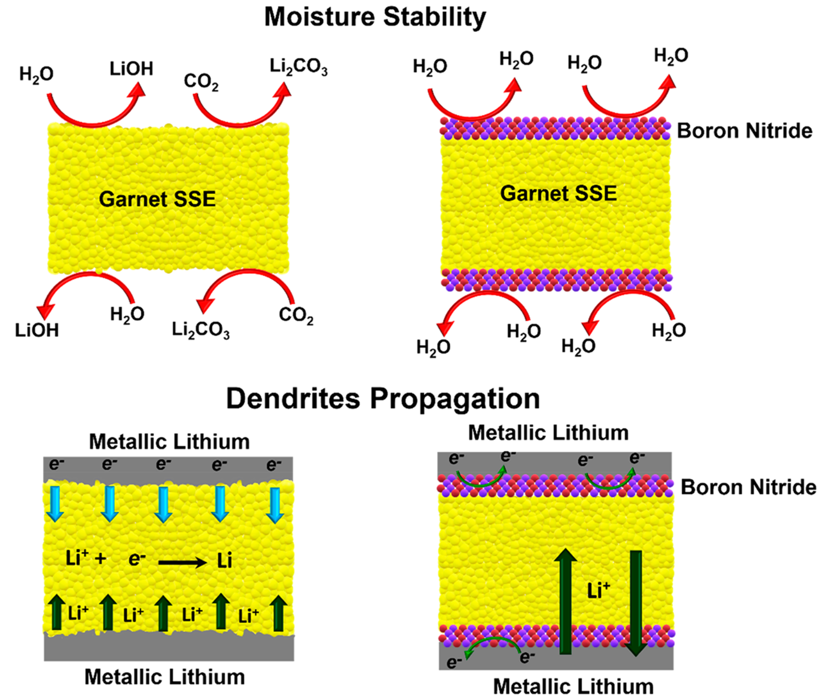

Figure 1. Schematic of surface-engineered garnet-type SSEs for moisture stability, improved wettability, and a dendrite-free system for better lithium ion transport across the interface.

The high electronic conductivity of the garnet-type SSE (10^{-8}–10^{-7} S cm^{-1}) was found to be responsible for the easy propagation of Li dendrites.[29] The mechanism of such a phenomenon was attributed to the leakage of a small amount of electrons into the electrolyte that combines with the Li ions to form metallic and dead Li inside the garnet-type SSE.[29] The formation of Li dendrites causes cell failure due to an internal short circuit and also leads to the low utilization of the Li metal anode, while the dead Li contributes to the Li anode loss as well.[30]

To address the above-mentioned issues, various approaches have been proposed, among which, introducing a transition layer at the electrode–electrolyte interface is considered to be an effective solution.[31] Previously, various types of materials like metals,[32,33] semiconductors,[7,34,35] insulators,[19,36] polymers,[37,38] etc. were utilized as interlayers, which successfully reduced the interfacial resistance and improved the wettability of Li. However, while the use of various interlayer coatings improves the performance, the fundamental working mechanisms that mitigate the interfacial resistance have certain pitfalls. For instance, metal interlayers are electronic conductors that can boost the flow of electrons into the garnet-type SSE, leading to the propagation of Li dendrites. Recent explorations of semiconductor-based materials indicate that alloy and conversion-based compounds contribute to Li alloying and conversion reactions that could lead to unfavorable passivation and volume changes that can induce cracks at the SSE surface and reduce Li-ion conductivity.[39] Hence, it is imperative to design an interlayer material that has the following key properties: (i) be electronically insulating in nature to prevent Li dendrite formation, (ii) should not hinder the Li-ion movement, (iii) be hydrophobic in nature so that it can enhance the resistance toward moisture, and (iv) should be inert with Li metal anodes, in order to solve the garnet-type SSE issues. Herein, we effectively address all the major challenges of garnet-type SSEs by introducing an insulating, hydrophobic boron nitride (h-BN) interlayer with high Young's modulus and dielectric constant to (i) protect the garnet solid electrolytes against metallic Li, (ii) form a chemically and mechanically stable interface, and (iii) provide an electronically insulating but ionically conducting anode interface, as depicted in Figure 1. For this purpose, we have shown the interlayer functionality of h-BN and its interaction with garnet electrolyte/metallic Li interface using in situ and ex situ spectroscopic studies and detailed electrochemical analysis. Detailed characterization elucidates that h-BN coatings on the LLZT surface make it resistant to the moisture-containing environment and provide a highly stable interface for Li plating/stripping with minimal polarization resistance that holds the key for developing efficient solid-state electrolytes for ASSBs.

RESULTS AND DISCUSSION

A garnet-type electrolyte with nominal composition of $Li_{6.5}La_3Zr_{1.5}Ta_{0.5}O_{12}$ (LLZT) was synthesized using a conventional solid-state synthesis method, followed by sintering at 1160 °C for 16 h (detailed synthesis procedure is provided in SI). Herein, 0.5% Ta substitution in $Li_7La_3Zr_2O_{12}$ (LLZO) was used to enhance its cubic phase stability.[40] Figure S1(a) represents the powder X-ray diffraction pattern (XRD) of the sintered LLZT pellet that matches well with the cubic garnet-type $Li_5La_3Nb_2O_{12}$ (PDF 80-0457). The relative density of the sintered LLZT pellet was determined to be 91% of the theoretical density. Further, as shown in Figure S1(b), the Raman spectra of LLZT match the characteristic peaks of the cubic garnet-type LLZT. The Raman band at 125 (E_g) cm^{-1} is attributed to the typical vibration of bulky La cations, and the two Raman peaks at 243 (A_{1g}) and 375 (T_{2g}) cm^{-1} correspond to the Li–O bonding. Here, it is noteworthy to mention that no apparent peak splitting was observed in the low-frequency regions, i.e., at 125, between 361 (T_{2g}) and 410 (E_g/T_{2g}), and

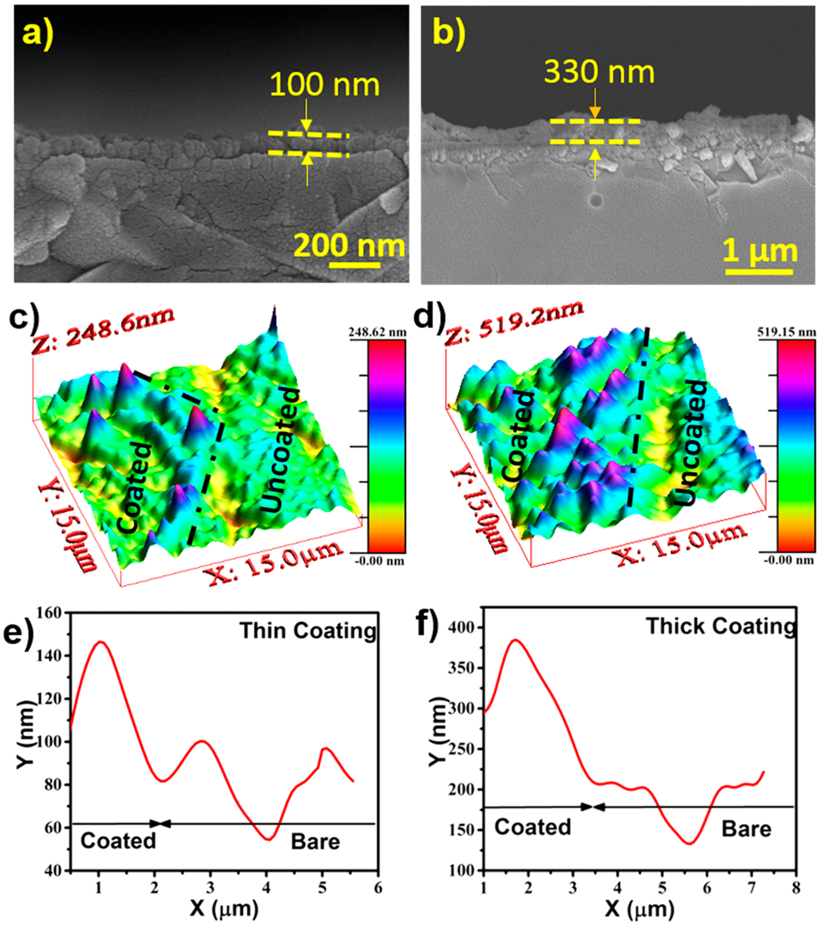

Figure 2. (a, b) FE-SEM cross-section images of a thin and thick coating of h-BN on LLZT. (c, d) AFM scan of the thin and thick h-BN coating on LLZT. (e, f) Corresponding AFM height profiles.

at 514 (T_{2g}/E_g) cm^{-1}, which indicates pure cubic garnet structure.[25,41] Figure S1(c) shows a cross-sectional morphology view of the LLZT pellet by using field emission scanning electron microscopy (FE-SEM), which shows a densely packed structure with an average grain size of 12 μm. The inset of Figure S1(c) shows the digital image of the polished, translucent LLZT pellet with a thickness of about 200 μm. The Li-ion conductivity of a cubic-faced LLZT was measured using electrochemical impedance spectroscopy (EIS) by the blocking-electrode method, as shown in Figure S1(d). The measured room-temperature Li-ion conductivity was found to be 4.13×10^{-4} S cm^{-1} at room temperature, which is in good agreement with the previous reports.[42] The capacitive behavior seen in the EIS plot is due to the gold blocking electrodes that behave like capacitors. The pellets were then stored in an argon-filled glovebox (oxygen, moisture < 0.1 ppm) for the subsequent experiments.

The h-BN, also known as "white graphene", is an electrical insulator with a very large bandgap >6 eV and high dielectric constant. The structure of h-BN is similar to graphene with alternate covalent sp^2 double bonds between the boron and nitrogen atoms, arranged like a honeycomb structure.[43] These planes are highly polarized due to the immense asymmetry of sublattices, which leads to a very large band gap.[44] This unique bonding leads to excellent resistance to oxidation and corrosion, and it exhibits excellent mechanical properties, such as flexibility, chemical inertness, unique electrochemical properties, etc.[45−48] The h-BN coating on the LLZT was achieved by a spray coating technique (Figure S2(c)) which is commercially viable, and scalable compared to other expensive and sophisticated methods like the atomic layer deposition, chemical vapor deposition, molecular beam epitaxy, etc.[49] For coating purposes, we utilized exfoliated h-BN nanosheets, which were prepared according to our previously reported studies.[50] Before the deposition of h-BN on LLZT, the samples were subjected to standard characterization. As shown in Figure S2(a), the translucent dispersion shows uniform distribution of the exfoliated h-BN nanosheets in 2-propanol solvent, which was then subjected to transmission electron microscopy (TEM) studies. The high-resolution TEM image in Figure S2(b) shows exfoliated nanosheets with wrinkled edges that indicate successful exfoliation. This can be attributed to weak van der Waals forces between the h-BN planes, which enable easy exfoliation of bulk h-BN into two-dimensional nanosheets. Later, to study the effect of coating thickness on the plating/stripping behavior, conformal coating of h-BN nanosheets was carried out on the garnet SSE surface with different thicknesses by varying the spraying time. The SSE pellets were labeled according to the thickness of the h-BN layer as thin and thick h-BN LLZT. The cross-sectional FE-SEM images (Figure 2(a,b)) depict uniform, conformal coating of h-BN on the LLZT surface. The thickness of the h-BN coatings on LLZT was found to be 100 and 330 nm for one- and three-second spray-coated LLZT, respectively.

The thickness of the h-BN coating was further verified using atomic force microscopy (AFM), as shown in Figures 2(c, d)

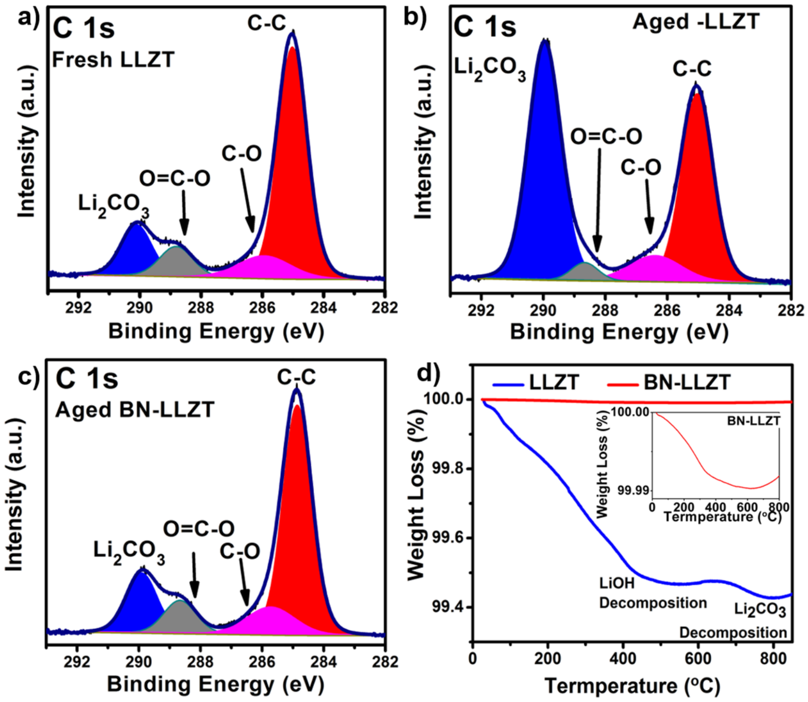

Figure 3. XPS C 1s analysis of the (a) as-prepared LLZT, (b) 120 h aged LLZT, and (c) aged h-BN-coated LLZT. (d) TGA analysis of aged LLZT and aged h-BN-coated LLZT pellets, the inset shows the zoomed part of the weight loss occurence in aged h-BN coated LLZT sample.

and S3. The line scanning was performed on uncoated LLZT, which reveals an average height of 60 nm. The line-like structures on the AFM scan are caused by the roughness of the emery paper used for polishing. The line scan over the thin h-BN coating reveals a height profile of 147 nm, while after subtracting the height profile of bare LLZT, the thickness of the coating was found to be approximately 87 nm, which is in accordance with the coating thickness obtained through the FE-SEM images. Similarly, the AFM image of the thick h-BN coating reveals a height of 330 nm, which is also following the FE-SEM image.

Further, the roughness analysis of the h-BN-coated and uncoated LLZT revealed that the h-BN-coated LLZT had a rougher surface with an average height of 85 and 218 nm for the 90 and 330 nm thick coatings, respectively, as shown in Figure S4. Whereas, the uncoated LLZT had a less rough surface with an average height of 56 nm, which is also evident with the height profile shown in Figure S3. Further, the size of the valleys (in between two positive deviations) along the x-axis is in the nanoscale (Figure S3(b)) for the uncoated LLZT, resulting in very sharp spikes that increase interfacial resistance owing to its poor wetting property, whereas the size of the valley is drastically increased in several orders (micron scale) in the case of h-BN-coated LLZT (Figure 2), which enhances its wetting property. Hence, the higher roughness of the h-BN coating in our case promotes better contact of the anode with the electrolyte that, in turn, reduces the interfacial resistance further; in contrast, the lower surface roughness in the uncoated LLZT makes it difficult for the Li metal to contact the LLZT pellet.[32] The uniformity of the h-BN coating was analyzed using FE-SEM by coating h-BN after masking half of the LLZT pellet using Kapton tape. Both the thin and thick coatings were found to be highly uniform, as shown in Figure S5(a,b), where the top portion is coated, while the bottom is uncoated LLZT. After the h-BN coating, the spray-coated LLZT was analyzed using Raman spectroscopy (Figure S6) to ensure that no structural changes occurred during the spray coating process. The Raman intensity at 1360 cm^{-1} corresponds to the exfoliated h-BN, and the other peaks correspond to that of LLZT.

In order to corroborate the moisture stability of the h-BN-coated LLZT, we have performed X-ray photoelectron spectroscopy (XPS) and thermal gravimetric analysis (TGA) on samples in fresh and aged conditions (120 h exposed to ambient atmospheric conditions), as shown in Figure 3. For a better comparison, uncoated LLZT pellets were aged simultaneously to ensure that identical environmental conditions were maintained for the pellets and analyzed in the same way. Figure 3(a) shows the deconvoluted XPS C 1s spectrum of fresh LLZT, which consists of two dominant peaks at 290 eV (blue) and 285.5 eV (red), corresponding to the Li_2CO_3 and adventitious carbon, respectively. The other peaks at 288.6 and 285.7 eV correspond to the carboxyl and hydroxyl groups present on the surface, respectively. The presence of a small amount of Li_2CO_3 on the fresh pellets can be attributed to the atmospheric synthesis and polishing conditions. After atmospheric exposure of uncoated LLZT pellets, the peak intensity of Li_2CO_3 was found to be increased drastically (Figure 3(b)), which indicates the growth of the carbonate species on the solid electrolyte surface. In contrast, insignificant changes were observed in the Li_2CO_3 peak intensity of the aged h-BN-coated LLZT (Figure 3(c)). The ratio of the carbonate to the adventitious carbon peak is 26.27% for the fresh LLZT and 28.94% for the aged thin h-BN-coated LLZT pellet, whereas it is 121.86% for the uncoated LLZT pellet. The observed XPS analysis corroborates the effectiveness of h-BN coating in suppressing the Li_2CO_3 formation on the garnet surface. This can be attributed to the inherent hydrophobic property of h-BN (contact angle of 125°) arising from its microroughness and surface en-

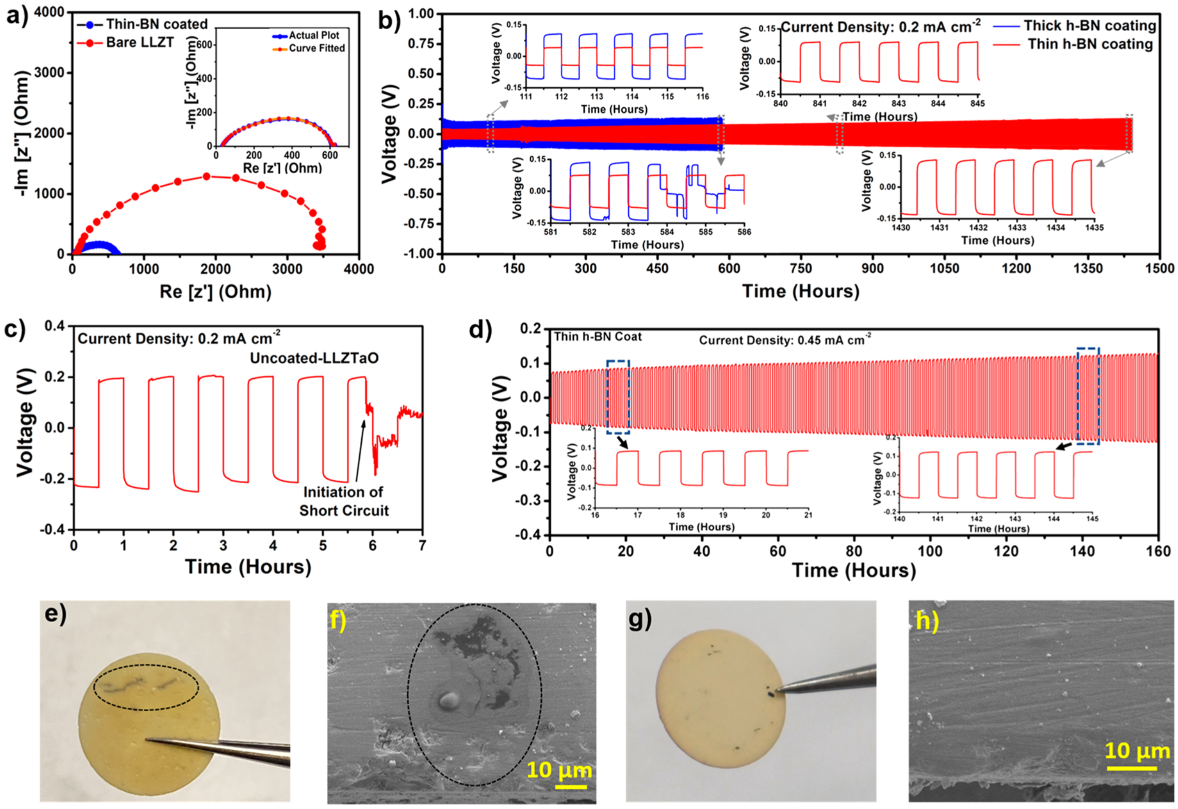

Figure 4. (a) Comparison of EIS profiles of the uncoated and thin-h-BN-coated LLZT symmetrical cells, measured at 22 °C, the zoomed EIS of the thin-h-BN coated LLZT cell is shown in the inset along with its corresponding curve fitting. (b−d) Galvanostatic cycling comparison of (b) thin and thick h-BN-coated LLZT symmetrical cells, (c) uncoated LLZT symmetrical cell, and (d) thin h-BN-coated LLZT at higher current density. All galvonostatic cycling experiments were done at 60 °C. (e−h) Post mortem analysis of galvanostatically cycled cell with (e, f) uncoated LLZT pellet, and (g, h) h-BN-coated LLZT pellet.

ergy.[43,51,52] Thus, hydrophobic h-BN effectively resists the interaction of moisture with the LLZT surface and hence prevents the H^+/Li^+ interchange reactions and associated degradation in moisture-containing environment. To further validate, the interaction between a water droplet and the h-BN-coated and uncoated LLZT pellet was performed, as shown in Supporting Information videos 1 and 2. It is well evident that the h-BN blocks the interaction between h-BN-coated LLZT pellet and the water droplet, whereas the uncoated LLZT pellet readily attracts it. To further analyze the long-term moisture exposure, comparison of a powder XRD pattern of the fresh and the 90-day-aged samples of bare LLZT and thin h-BN-coated LLZT was carried out to demonstrate the protective nature of the h-BN coating. As evident from Figure S7, there is a significant increase in the peaks marked with "β" in the aged samples of uncoated LLZT, which corresponds to Li_2CO_3.[53] There is no appearance of such peaks in the aged samples of thin h-BN-coated samples, indicating suppression of Li_2CO_3 even after 90 days. To quantify the atmospheric effect on LLZT, we have performed a thermogravimetric (TGA) analysis of the aged uncoated and thin h-BN-coated LLZT, as shown in Figure 3(d). The aged uncoated LLZT showed 0.6% weight loss in two major regions. The weight loss at ~450 °C corresponds to the decomposition of LiOH formed due to the hydration of LLZT (Li^+/H^+ exchange) (eq 1). The weight loss at ~700 °C corresponds to the loss of carbon dioxide (CO_2) through the decomposition of Li_2CO_3 that is formed by the reaction of CO_2 with lithium hydroxide (eq 2). However, there is only an insignificant weight loss (0.01%, as shown in inset Figure 3(d)) in the aged h-BN-coated LLZT samples, which may be due to the pre-existing Li_2CO_3 in the fresh samples.

In order to gauge the effect of h-BN coating on the interfacial resistance of LLZT, we have performed electrochemical impedance spectroscopy (EIS) studies on a symmetric Li|garnet|Li cell at 22 °C, as shown in Figure 4(a). The inset shows the curve fitting of the EIS spectra obtained from the h-BN-coated symmetrical cell, and the corresponding equivalent circuit is shown in Figure S8. Symmetric cells were assembled by attaching Li metal foil on both sides of the uncoated and the h-BN-coated LLZT. These symmetrical cells were heated at 185 °C on a hot plate for 2 h in a stainless-steel (SS) crucible under a small load applied by placing four SS discs (6 g) on the top to ensure adequate adhesion between the electrodes. After heating, the cells were transferred to a custom-made Swagelok-type cell that can apply high pressure (126 kPa) on symmetrical cells, which ensures better contact for electrochemical evaluation. The interfacial impedances were calculated by subtracting the total cell resistance of the symmetrical cell by the electrolyte resistance obtained from the blocking electrode method (Au|LLZTaO|Au) and dividing the value by two as there are two interfaces involved in a symmetrical cell. The interfacial resistance was calculated as 1660 Ω cm^2 and 220 Ω cm^2 at 22 °C for the uncoated and thin h-BN-coated LLZT, respectively. The reduction in the interfacial impedance evidenced that the h-BN coating effectively mitigates the hindrance for the Li-ion transport across the metallic Li/LLZT interface. The observed interfacial effect can be due to the interaction of h-BN with

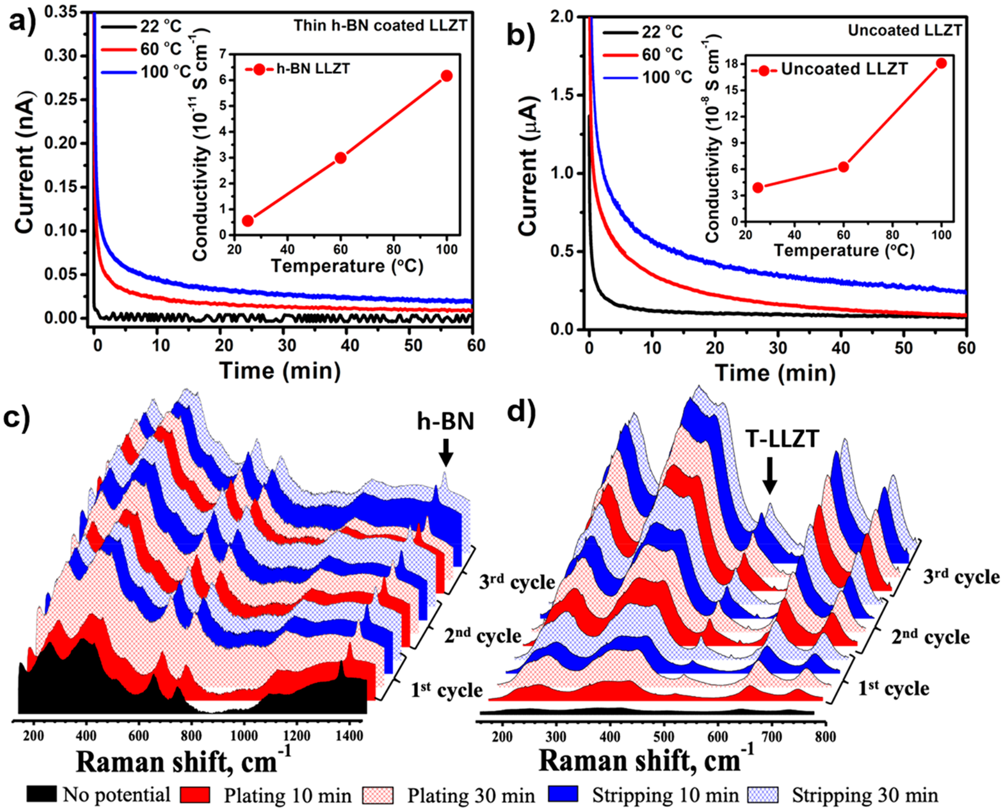

Figure 5. Electronic conductivity measurements of (a) h-BN-coated LLZT and (b) uncoated LLZT at different temperatures, inset shows the variation of electronic conductivity with temperature. In situ Raman analysis during galvostatic plating/stripping of (c) h-BN-coated and (d) uncoated LLZT.

metallic Li through weak van der Waals forces, as predicted by first-principle methods.[54] Further, the electron-deficient boron atom in h-BN interacts with electron-rich Li via the Lewis acid−base approach, which aids the hopping of Li ions across the h-BN-coated interface. Also, the point defects present in the h-BN lattice allow Li ions to pass through the solid electrode/electrolyte interface.[50,55,56] Previously reported work on using h-BN−lithium composite anode explored the effect of wettability of the anode with garnet-type SSE.[57] However, this method cannot incorporate moisture stability to the SSE and also fail to prevent the leakage of electrons into the SSE.

The assembled symmetrical cell was subjected to typical galvanostatic charge/discharge cycle testing to evaluate Li-ion transport by applying 0.2 mA/cm^2 current density with a periodic 1 h charge/discharge cycle, as shown in Figure 4(b). As expected, the thin h-BN-coated LLZT interface delivered a stable Li-ion plating/stripping behavior for 1400 cycles (i.e., 1400 h) at 60 °C with a minimal overpotential. The insets demonstrate the stability of Li plating/stripping behavior without any noise in the signal, despite a slight increment in the voltage hysteresis. EIS measurements were performed on this cell after 1000 cycles and the results were compared with that of a fresh cell before subjecting it for further cycling, as shown in Figure S9. As observed from the EIS plot, interfacial impedance increased slightly after 1000 cycles; however, the garnet electrolyte bulk resistance remains the same in the tested cells. This result reveals that h-BN coating effectively protects the garnet electrolyte from metallic Li-ion-induced interfacial changes when they are in direct contact, as observed in other cases.[58] The obtained results indicate that the h-BN-coated LLZT interface provides an excellent pathway for the smooth transport of Li ions and, more importantly, effectively preventsthe formation and propagation of Li dendrites.

In contrast, as shown in Figure 4(c), the uncoated garnet (Li|LLZT|Li) cell showed a large overpotential of 0.2 V and shorted in 6 h at a current density of 0.2 mA cm^{-2} because of the Li dendrite propagation across the SSE interface at 60 °C. This can be attributed to an uneven current distribution across the surface, which is predominantly caused by the presence of the Li-ion transport limiting Li_2CO_3 layer on the LLZT surface.[59] Figure 4(d) shows the cycling behavior of h-BN-coated LLZT symmetrical cells at a higher current density of 0.45 mA cm^{-2}, and reveals that the cell shows a small voltage hysteresis window along with excellent stability even at higher current density. Similarly, to verify the role of h-BN thickness on the lithium plating/stripping behavior , we evaluated the 300 nm thick h-BN-coated LLZT symmetrical cell (shown in Figure 4(b), blue curve). The cell showed a stable Li plating/stripping tendency for 583 h at a current density of 0.2 mA cm^{-2} with an overpotential of 0.090 V before it shorted, which demontrates the capablity of thick coated h-BN in Li-ion transport across the interface. The stable Li plating/stripping behavior for more than 1400 h with h-BN coating can be ascribed to its insulating nature (electronic conductivity in the order of 10^{-15} S cm^{-1}) that ideally blocks the electron leakage across the interface and electronically isolates the LLZT, which prevents the formation of Li dendrites.[60] Further, the very high Young's modulus character of h-BN (1 TPa) aids in curbing the propagation of Li dendrites.[48] In addition, the critical current density was found to be 0.25 and 0.65 mA cm^{-2} for the uncoated and the h-BN-coated LLZT, respectively (Figure S10). The improvement in the critical current density is certainly attributed to the inhibition of Li dendrite formation by the h-BN interlayer. It is widely accepted that inhomogeneous contact between Li and garnet leads to uneven Li-ion flux/transport during Li plating/stripping, which are the predominant factors influencing the dendrite formation and increase in interfacial resistance values. In our case, the conformal coatings of h-BN on the LLZT homogeneously provide uniform contact that results in controlled Li-ion flux and even current distribution on electrodes during operation.

The post-mortem analysis of the uncoated LLZT cell revealed the propagation of Li dendrites through the uncoated LLZT after six cycles (Figure 4(e, f)). The dark lines (encircled) observed in Figure 4(e) show the trajectory of the lithium spots, through which the Li dendrites propagated and leads to the short-circuiting of the cell. The corresponding cross-sectional FE-SEM image (Figure 4(f)) of the trajectory revealed metallic deposits of lithium metal in the uncoated LLZT pellet, encircled in black dashed curves. However, no such formation was observed in the thin h-BN-coated LLZT even after 1000 h of cycling (Figure 4(g, h)). The tiny black spots, as seen in Figure 4(g), are due to the partial oxidation of lithium metal fragments that stick to the LLZT surface after scrapping the lithium metal out of the cycled symmetrical cells. However, the cross-section of the FE-SEM image of the cycled thin h-BN-LLZT does not show any such internal Li metal deposits.

To understand the role of h-BN as an interlayer between LLZT and metallic Li, we performed in situ Raman spectroscopy and electronic conductivity experiments on the uncoated and thin h-BN-coated LLZT. As an alloying reaction governs the interfacial process, the volume expansion becomes unavoidable in the case of metal/metallic oxide-based interlayers, which paves a way for damaging the contact between the metallic Li and garnet SSE. Figure 5(a) shows chronoamperometry measurements to elucidate the effect of h-BN coating on the electronic conductivity at the interface. The conductivity measurement cells were made by sputtering gold on either side of the uncoated and h-BN-coated LLZT pellets. In this approach, a constant voltage is applied versus the open-circuit potential (OCP), and a resultant steady-state current (I_s) is obtained. Then, the electronic conductivity is calculated from chronoamperometry curve using eq 3, where σ is the electronic conductivity of the pellet; l is the thickness of the pellet in cm; A is the area of the pellet in cm^2; I is the steady-state current obtained; and E is the constant potential applied.

$$\sigma = \frac{ldI}{AdE} \tag{3}$$

The thin BN coating on LLZT drastically lowered the electronic conductivity of the pellet from 3.8×10^{-8} to 5.5×10^{-12} S cm^{-1} at 22 °C. This drastic reduction in the value of electronic conductivity of the SSE can be attributed to the insulating nature and the very high bandgap of the h-BN interlayer. By examining the electronic conductivity at various temperatures, it was observed that the electronic conductivity increases with temperature due to the increase in randomness within the solid electrolyte. The higher electronic conductivity of garnet-type SSEs permits relatively "free" electron transfer across the interface, where the electrons can be trapped at the pore/crack surfaces and grain boundaries, which leads to the propagation of Li dendrites upon reduction of Li ions.[61] In our case, the h-BN-coated LLZT showed electronic conductivity almost three orders less than the uncoated LLZT, which implies that the h-BN coatings can effectively improve the critical current density values of garnet SSE.

Though several surface coatings[19,62−64] were implemented to enhance the performance of the ASSBs, a fundamental understanding of the degradation behavior of the interlayers still remains unknown and poses serious concerns regarding their practical applicability.[65] Further, given the fact that the Li metal anode is highly reductive in nature toward these interlayers,[66] it is particularly important to visualize their stability, especially on the Li side. To demonstrate the stability of the h-BN interlayer over several Li plating and stripping cycles, we performed systematic in situ Raman spectroscopy analysis at the Li|h-BN|LLZT interface. A homemade, 3D-printed in situ symmetrical cell setup attached with a microheater (Figure S11) was developed for this purpose, and in situ Raman studies were conducted under an inert atmosphere using a specially designed transfer chamber as described in our previous report.[67] Herein, the Raman laser was focused on the interface along with the h-BN interlayer that is present between the Li and the LLZT in the cross-section of the symmetrical cell, as shown in Figure S11. Figure 5(c, d) shows the recorded in situ Raman spectrum of the h-BN-coated and uncoated LLZT interfaces to monitor metallic Li-induced chemical changes across the h-BN-coated interface. The in situ Raman spectrum at the initiation of the experiment displayed typical Raman bands of LLZT at 127 (E_g), 243, 410 (T_{2g}), 642, and 744 cm^{-1} and h-BN at 1360 cm^{-1}. The Li plating and stripping process was carried out for 30 min each, and Raman spectra were recorded every 10 min. During the plating and stripping of Li over three subsequent cycles, the Raman band of h-BN at 1360 cm^{-1} did not show any signs of spectral changes, indicating the robustness of the h-BN interlayer against metallic Li. Besides, no significant changes were observed in the Raman bands of the cubic LLZT sample, indicating that the material does not undergo any structural or chemical transformation during the cycling. The high stability of the h-BN layer at the anode interface can be attributed to the property of nitrides, which are highly stable against reductive decomposition and possess the largest cohesive energy that makes them highly stable at the interface.[68] On the other hand, the Raman spectrum of the uncoated LLZT (Figure 5(d)) displayed characteristic LLZT Raman bands at the initiation of the cycling studies. However, as cycling progressed, the emergence of a new peak was observed at ~500 cm^{-1} (as indicated by a black arrow), and a peak splitting was observed at the Li$^+$ ion bonding sensitive region between 361 and 410 cm^{-1}. The emergence of a new peak and peak splitting usually occurs during the structural phase transformation from the pure cubic to the tetragonal phase of LLZT. This may be due to the fact that the highly reductive Li metal when in contact with LLZT spontaneously reduces the LLZT, thus forming a tetragonal phase.[66] Tetragonal LLZT inherently possesses lower ionic conductivity, which may lead to an increase in the interfacial resistance.[69]

■ CONCLUSION

In this study, we demonstrated a two-dimensional material-based interlayer approach to mitigate various interfacial issues of the garnet-type SSE. The conformal interlayer coatings of two-dimensional h-BN nanosheets on garnet-type SSE were achieved through a cost-effective spray coating method. Detailed spectroscopic evidence revealed that h-BN nanosheet-coated LLZT exhibited excellent stability in moisture conditions for over 120 h and restricted the formation of Li_2CO_3 layers. Further, h-BN coatings drastically reduced the LLZT interfacial impedance as a consequence of Lewis acid−base interaction between the h-BN and Li metal. The highly insulating property of h-BN effectively blocked the passage of the electrons from Li metal into the LLZT, which results in mitigation of dendrites formation as evidenced from the stable plating/stripping behavior over 1400 cycles at 60 °C, at a current density of 0.2 mA cm^{-2}. In situ Raman analysis revealed a noninteracting, stable interlayer that prevented the growth of the tetragonal phase of LLZT at the interphase of Li and LLZT and demonstrates the robustness of h-BN interlayer in protecting garnet surface against highly reductive metallic lithium. It is anticipated that the proposed two-dimensional nanosheets-based strategy opens a new avenue to resolve the interfacial issues of garnet-type SSEs.

■ ASSOCIATED CONTENT

Supporting Information

The Supporting Information is available free of charge at https://pubs.acs.org/doi/10.1021/acsaem.0c00905.

Experimental details, characterization of the as-synthesized LLZO samples, AFM roughness analysis, XRD evaluation of moisture studies, in situ cell assembly, etc. (PDF)

Wetting property of h-BN-coated LLZT (MP4)

Wetting property of uncoated LLZT (MP4)

■ AUTHOR INFORMATION

Corresponding Author

Leela Mohana Reddy Arava − *Department of Mechanical Engineering, Wayne State University, Detroit, Michigan 48202, United States;* orcid.org/0000-0001-6685-6061; Email: leela.arava@wayne.edu

Authors

Sathish Rajendran − *Department of Mechanical Engineering, Wayne State University, Detroit, Michigan 48202, United States*

Naresh Kumar Thangavel − *Department of Mechanical Engineering, Wayne State University, Detroit, Michigan 48202, United States*

Kiran Mahankali − *Department of Mechanical Engineering, Wayne State University, Detroit, Michigan 48202, United States;* orcid.org/0000-0003-3540-5350

Complete contact information is available at: https://pubs.acs.org/10.1021/acsaem.0c00905

Notes

The authors declare no competing financial interest.

■ ACKNOWLEDGMENTS

This material is based upon work supported by the National Science Foundation under Grant No. 1751472. The authors thank the Lumigen Instrument Centre at Wayne State University for the use of PXRD (NSF:MRI 1427926), JEOL TEM (NSF:MRI 0216084), and FE-SEM (NSF:MRI 0922912) facilities.

■ REFERENCES

(1) Whittingham, M. S. Ultimate limits to intercalation reactions for lithium batteries. *Chem. Rev.* **2014**, *114* (23), 11414−43.

(2) Armand, M.; Tarascon, J. M. Building better batteries. *Nature* **2008**, *451* (7179), 652−7.

(3) Goodenough, J. B.; Kim, Y. Challenges for rechargeable Li batteries. *Chem. Mater.* **2010**, *22* (3), 587−603.

(4) Park, K.; Yu, B. C.; Jung, J. W.; Li, Y. T.; Zhou, W. D.; Gao, H. C.; Son, S.; Goodenough, J. B. Electrochemical Nature of the Cathode Interface for a Solid-State Lithium-Ion Battery: Interface between LiCoO2 and Garnet-Li7La3Zr2O12. *Chem. Mater.* **2016**, *28* (21), 8051−8059.

(5) O'Callaghan, M. P.; Powell, A. S.; Titman, J. J.; Chen, G. Z.; Cussen, E. J. Switching on Fast Lithium Ion Conductivity in Garnets: The Structure and Transport Properties of Li3+ x Nd3Te2− x Sb x O12. *Chem. Mater.* **2008**, *20* (6), 2360−2369.

(6) Jin, Y.; Liu, K.; Lang, J. L.; Zhuo, D.; Huang, Z. Y.; Wang, C. A.; Wu, H.; Cui, Y. An intermediate temperature garnet-type solid electrolyte-based molten lithium battery for grid energy storage. *Nat. Energy* **2018**, *3* (9), 732−738.

(7) Wang, C.; Gong, Y.; Liu, B.; Fu, K.; Yao, Y.; Hitz, E.; Li, Y.; Dai, J.; Xu, S.; Luo, W.; Wachsman, E. D.; Hu, L. Conformal, Nanoscale ZnO Surface Modification of Garnet-Based Solid-State Electrolyte for Lithium Metal Anodes. *Nano Lett.* **2017**, *17* (1), 565−571.

(8) Xu, X.; Takada, K.; Watanabe, K.; Sakaguchi, I.; Akatsuka, K.; Hang, B. T.; Ohnishi, T.; Sasaki, T. Self-organized core−shell structure for high-power electrode in solid-state lithium batteries. *Chem. Mater.* **2011**, *23* (17), 3798−3804.

(9) Buschmann, H.; Dölle, J.; Berendts, S.; Kuhn, A.; Bottke, P.; Wilkening, M.; Heitjans, P.; Senyshyn, A.; Ehrenberg, H.; Lotnyk, A.; et al. Structure and dynamics of the fast lithium ion conductor "Li 7 La 3 Zr 2 O 12. *Phys. Chem. Chem. Phys.* **2011**, *13* (43), 19378−19392.

(10) Murugan, R.; Thangadurai, V.; Weppner, W. Fast lithium ion conduction in garnet-type Li7La3Zr2O12. *Angew. Chem., Int. Ed.* **2007**, *46* (41), 7778−7781.

(11) Kamaya, N.; Homma, K.; Yamakawa, Y.; Hirayama, M.; Kanno, R.; Yonemura, M.; Kamiyama, T.; Kato, Y.; Hama, S.; Kawamoto, K. A lithium superionic conductor. *Nat. Mater.* **2011**, *10* (9), 682.

(12) Ihlefeld, J. F.; Clem, P. G.; Doyle, B. L.; Kotula, P. G.; Fenton, K. R.; Applett, C. A. Fast Lithium-Ion Conducting Thin-Film Electrolytes Integrated Directly on Flexible Substrates for High-Power Solid-State Batteries. *Adv. Mater.* **2011**, *23* (47), 5663−5667.

(13) Lü, X.; Howard, J. W.; Chen, A.; Zhu, J.; Li, S.; Wu, G.; Dowden, P.; Xu, H.; Zhao, Y.; Jia, Q. Antiperovskite Li3OCl Superionic Conductor Films for Solid-State Li-Ion Batteries. *Adv. Sci.* **2016**, *3* (3), 1500359.

(14) Feng, J. K.; Yan, B.; Liu, J.; Lai, M.; Li, L. All solid state lithium ion rechargeable batteries using NASICON structured electrolyte. *Mater. Technol.* **2013**, *28* (5), 276−279.

(15) Noguchi, Y.; Kobayashi, E.; Plashnitsa, L. S.; Okada, S.; Yamaki, J.-i. Fabrication and performances of all solid-state symmetric sodium battery based on NASICON-related compounds. *Electrochim. Acta* **2013**, *101*, 59−65.

(16) Thangadurai, V.; Pinzaru, D.; Narayanan, S.; Baral, A. K. Fast solid-state Li ion conducting garnet-type structure metal oxides for energy storage. *J. Phys. Chem. Lett.* **2015**, *6* (2), 292−299.

(17) Kato, T.; Hamanaka, T.; Yamamoto, K.; Hirayama, T.; Sagane, F.; Motoyama, M.; Iriyama, Y. In-situ Li7La3Zr2O12/LiCoO2 interface modification for advanced all-solid-state battery. *J. Power Sources* **2014**, *260*, 292−298.

(18) Ohta, S.; Komagata, S.; Seki, J.; Saeki, T.; Morishita, S.; Asaoka, T. All-solid-state lithium ion battery using garnet-type oxide and Li3BO3 solid electrolytes fabricated by screen-printing. *J. Power Sources* **2013**, *238*, 53−56.

(19) Han, X.; Gong, Y.; Fu, K. K.; He, X.; Hitz, G. T.; Dai, J.; Pearse, A.; Liu, B.; Wang, H.; Rubloff, G.; et al. Negating interfacial impedance in garnet-based solid-state Li metal batteries. *Nat. Mater.* **2017**, *16* (5), 572.

(20) Aguesse, F.; Manalastas, W.; Buannic, L.; Lopez Del Amo, J. M.; Singh, G.; Llordes, A.; Kilner, J. Investigating the Dendritic Growth during Full Cell Cycling of Garnet Electrolyte in Direct Contact with Li Metal. *ACS Appl. Mater. Interfaces* **2017**, *9* (4), 3808−3816.

(21) Cheng, E. J.; Sharafi, A.; Sakamoto, J. Intergranular Li metal propagation through polycrystalline Li6. 25Al0. 25La3Zr2O12 ceramic electrolyte. *Electrochim. Acta* **2017**, *223*, 85−91.

(22) Galven, C.; Fourquet, J. L.; Crosnier-Lopez, M. P.; Le Berre, F. Instability of the Lithium Garnet Li7La3Sn2O12: Li+/H+ Exchange and Structural Study. *Chem. Mater.* **2011**, *23* (7), 1892−1900.

(23) Cheng, L.; Wu, C. H.; Jarry, A.; Chen, W.; Ye, Y. F.; Zhu, J. F.; Kostecki, R.; Persson, K.; Guo, J. H.; Salmeron, M.; Chen, G. Y.; Doeff, M. Interrelationships among Grain Size, Surface Composition, Air Stability, and Interfacial Resistance of Al-Substituted Li7La3Zr2O12 Solid Electrolytes. *ACS Appl. Mater. Interfaces* **2015**, *7* (32), 17649−17655.

(24) Brugge, R. H.; Hekselman, A. K. O.; Cavallaro, A.; Pesci, F. M.; Chater, R. J.; Kilner, J. A.; Aguadero, A. Garnet Electrolytes for Solid State Batteries: Visualization of Moisture-Induced Chemical Degradation and Revealing Its Impact on the Li-Ion Dynamics. *Chem. Mater.* **2018**, *30* (11), 3704−3713.

(25) Larraz, G.; Orera, A.; Sanjuan, M. Cubic phases of garnet-type Li 7 La 3 Zr 2 O 12: the role of hydration. *J. Mater. Chem. A* **2013**, *1* (37), 11419−11428.

(26) Jones, J. C.; Rajendran, S.; Pilli, A.; Lee, V.; Chugh, N.; Arava, L. M. R.; Kelber, J. A. In situ x-ray photoelectron spectroscopy study of lithium carbonate removal from garnet-type solid-state electrolyte using ultra high vacuum techniques. *J. Vac. Sci. Technol., A* **2020**, *38* (2), 023201.

(27) Li, Y.; Chen, X.; Dolocan, A.; Cui, Z.; Xin, S.; Xue, L.; Xu, H.; Park, K.; Goodenough, J. B. Garnet Electrolyte with an Ultralow Interfacial Resistance for Li-Metal Batteries. *J. Am. Chem. Soc.* **2018**, *140* (20), 6448−6455.

(28) Huo, H. Y.; Chen, Y.; Zhao, N.; Lin, X. T.; Luo, J.; Yang, X. F.; Liu, Y. L.; Guo, X. X.; Sun, X. L. In-situ formed Li2CO3-free garnet/Li interface by rapid acid treatment for dendrite-free solid-state batteries. *Nano Energy* **2019**, *61*, 119−125.

(29) Han, F. D.; Westover, A. S.; Yue, J.; Fan, X. L.; Wang, F.; Chi, M. F.; Leonard, D. N.; Dudney, N.; Wang, H.; Wang, C. S. High electronic conductivity as the origin of lithium dendrite formation within solid electrolytes. *Nat. Energy* **2019**, *4* (3), 187−196.

(30) Cheng, X.-B.; Zhao, C.-Z.; Yao, Y.-X.; Liu, H.; Zhang, Q. Recent advances in energy chemistry between solid-state electrolyte and safe lithium-metal anodes. *Chem.* **2019**, *5*, 74−96.

(31) Du, M. J.; Liao, K. M.; Lu, Q.; Shao, Z. P. Recent advances in the interface engineering of solid-state Li-ion batteries with artificial buffer layers: challenges, materials, construction, and characterization. *Energy Environ. Sci.* **2019**, *12* (6), 1780−1804.

(32) Fu, K. K.; Gong, Y.; Liu, B.; Zhu, Y.; Xu, S.; Yao, Y.; Luo, W.; Wang, C.; Lacey, S. D.; Dai, J.; Chen, Y.; Mo, Y.; Wachsman, E.; Hu, L. Toward garnet electrolyte-based Li metal batteries: An ultrathin, highly effective, artificial solid-state electrolyte/metallic Li interface. *Sci. Adv.* **2017**, 3 (4), e1601659.

(33) Fu, K. K.; Gong, Y.; Fu, Z.; Xie, H.; Yao, Y.; Liu, B.; Carter, M.; Wachsman, E.; Hu, L. Transient Behavior of the Metal Interface in Lithium Metal-Garnet Batteries. *Angew. Chem., Int. Ed.* **2017**, *56* (47), 14942−14947.

(34) Luo, W.; Gong, Y.; Zhu, Y.; Fu, K. K.; Dai, J.; Lacey, S. D.; Wang, C.; Liu, B.; Han, X.; Mo, Y.; Wachsman, E. D.; Hu, L. Transition from Superlithiophobicity to Superlithiophilicity of Garnet Solid-State Electrolyte. *J. Am. Chem. Soc.* **2016**, *138* (37), 12258−62.

(35) Fu, J. M.; Yu, P. F.; Zhang, N.; Ren, G. X.; Zheng, S.; Huang, W. C.; Long, X. H.; Li, H.; Liu, X. S. In situ formation of a bifunctional interlayer enabled by a conversion reaction to initiatively prevent lithium dendrites in a garnet solid electrolyte. *Energy Environ. Sci.* **2019**, *12* (4), 1404−1412.

(36) Xu, H. H.; Li, Y. T.; Zhou, A. J.; Wu, N.; Xin, S.; Li, Z. Y.; Goodenough, J. B. Li3N-Modified Garnet Electrolyte for All-Solid-State Lithium Metal Batteries Operated at 40 degrees C. *Nano Lett.* **2018**, *18* (11), 7414−7418.

(37) Xie, H.; Yang, C.; Fu, K.; Yao, Y.; Jiang, F.; Hitz, E.; Liu, B.; Wang, S.; Hu, L. Flexible, Scalable, and Highly Conductive Garnet-Polymer Solid Electrolyte Templated by Bacterial Cellulose. *Adv. Energy Mater.* **2018**, *8* (18), 1703474.

(38) Liu, B.; Gong, Y.; Fu, K.; Han, X.; Yao, Y.; Pastel, G.; Yang, C.; Xie, H.; Wachsman, E. D.; Hu, L. Garnet Solid Electrolyte Protected Li-Metal Batteries. *ACS Appl. Mater. Interfaces* **2017**, *9* (22), 18809−18815.

(39) Feng, W. L.; Dong, X. L.; Lai, Z. Z.; Zhang, X. Y.; Wang, Y. G.; Wang, C. X.; Luo, J. Y.; Xia, Y. Y. Building an Interfacial Framework: Li/Garnet Interface Stabilization through a Cu6Sn5 Layer. *ACS Energy Lett.* **2019**, *4* (7), 1725−1731.

(40) Thompson, T.; Wolfenstine, J.; Allen, J. L.; Johannes, M.; Huq, A.; David, I. N.; Sakamoto, J. Tetragonal vs. cubic phase stability in Al−free Ta doped Li 7 La 3 Zr 2 O 12 (LLZO). *J. Mater. Chem. A* **2014**, *2* (33), 13431−13436.

(41) Kumar, P. J.; Nishimura, K.; Senna, M.; Düvel, A.; Heitjans, P.; Kawaguchi, T.; Sakamoto, N.; Wakiya, N.; Suzuki, H. A novel low-temperature solid-state route for nanostructured cubic garnet Li 7 La 3 Zr 2 O 12 and its application to Li-ion battery. *RSC Adv.* **2016**, *6* (67), 62656−62667.

(42) Li, Y. T.; Han, J. T.; Wang, C. A.; Xie, H.; Goodenough, J. B. Optimizing Li+ conductivity in a garnet framework. *J. Mater. Chem.* **2012**, *22* (30), 15357−15361.

(43) Thangasamy, P.; Partheeban, T.; Sudanthiramoorthy, S.; Sathish, M. Enhanced superhydrophobic performance of BN-MoS2 heterostructure prepared via a rapid, one-pot supercritical fluid processing. *Langmuir* **2017**, *33* (24), 6159−6166.

(44) Zhang, K. L.; Feng, Y. L.; Wang, F.; Yang, Z. C.; Wang, J. Two dimensional hexagonal boron nitride (2D-hBN): synthesis, properties and applications. *J. Mater. Chem. C* **2017**, *5* (46), 11992−12022.

(45) Hasegawa, K.; Noda, S. Millimeter-Tall Single-Walled Carbon Nanotubes Rapidly Grown with and without Water. *ACS Nano* **2011**, *5* (2), 975−984.

(46) Wang, X.; Zhi, C.; Weng, Q.; Bando, Y.; Golberg, D. In Boron nitride nanosheets: novel syntheses and applications in polymeric composites. *J. of Physics: Conference Series*, IOP Publishing: 2013; p 012003.

(47) Bhimanapati, G.; Glavin, N.; Robinson, J. A. 2D Boron Nitride: Synthesis and Applications. In *Semiconductors and Semimetals*; Elsevier: 2016; Vol. *95*, pp 101−147.

(48) Falin, A.; Cai, Q.; Santos, E. J.; Scullion, D.; Qian, D.; Zhang, R.; Yang, Z.; Huang, S.; Watanabe, K.; Taniguchi, T.; et al. Mechanical properties of atomically thin boron nitride and the role of interlayer interactions. *Nat. Commun.* **2017**, *8*, 15815.

(49) Suo, L.; Borodin, O.; Gao, T.; Olguin, M.; Ho, J.; Fan, X.; Luo, C.; Wang, C.; Xu, K. "Water-in-salt" electrolyte enables high-voltage aqueous lithium-ion chemistries. *Science* **2015**, *350* (6263), 938−43.

(50) Babu, G.; Sawas, A.; Thangavel, N. K.; Arava, L. M. R. Two-Dimensional Material-Reinforced Separator for Li-Sulfur Battery. *J. Phys. Chem. C* **2018**, *122* (20), 10765−10772.

(51) Lei, W.; Portehault, D.; Liu, D.; Qin, S.; Chen, Y. Porous boron nitride nanosheets for effective water cleaning. *Nat. Commun.* **2013**, *4*, 1777.

(52) Zhou, Y.; Wang, Y.; Liu, T.; Xu, G.; Chen, G.; Li, H.; Liu, L.; Zhuo, Q.; Zhang, J.; Yan, C. Superhydrophobic hBN-regulated sponges with excellent absorbency fabricated using a green and facile method. *Sci. Rep.* **2017**, *7*, 45065.

(53) Vardar, G.; Bowman, W. J.; Lu, Q. Y.; Wang, J. Y.; Chater, R. J.; Aguadero, A.; Seibert, R.; Terry, J.; Hunt, A.; Waluyo, I.; Fong, D. D.; Jarry, A.; Crumlin, E. J.; Hellstrom, S. L.; Chiang, Y. M.; Yildiz, B. Structure, Chemistry, and Charge Transfer Resistance of the Interface between Li7La3Zr2O12 Electrolyte and LiCoO2 Cathode. *Chem. Mater.* **2018**, *30* (18), 6259−6276.

(54) Shi, L.; Xu, A.; Zhao, T. S. First-Principles Investigations of the Working Mechanism of 2D h-BN as an Interfacial Layer for the

Anode of Lithium Metal Batteries. *ACS Appl. Mater. Interfaces* **2017**, *9* (2), 1987−1994.

(55) Rodrigues, M. T. F.; Kalaga, K.; Gullapalli, H.; Babu, G.; Reddy, A. L. M.; Ajayan, P. M. Hexagonal Boron Nitride-Based Electrolyte Composite for Li-Ion Battery Operation from Room Temperature to 150° C. *Adv. Energy Mater.* **2016**, *6* (12), 1600218.

(56) Fan, Y.; Yang, Z.; Hua, W.; Liu, D.; Tao, T.; Rahman, M. M.; Lei, W.; Huang, S.; Chen, Y. Functionalized Boron Nitride Nanosheets/Graphene Interlayer for Fast and Long-Life Lithium−Sulfur Batteries. *Adv. Energy Mater.* **2017**, *7* (13), 1602380.

(57) Wen, J.; Huang, Y.; Duan, J.; Wu, Y.; Luo, W.; Zhou, L.; Hu, C.; Huang, L.; Zheng, X.; Yang, W.; Wen, Z.; Huang, Y. Highly Adhesive Li-BN Nanosheet Composite Anode with Excellent Interfacial Compatibility for Solid-State Li Metal Batteries. *ACS Nano* **2019**, *13* (12), 14549−14556.

(58) Ma, C.; Cheng, Y.; Yin, K.; Luo, J.; Sharafi, A.; Sakamoto, J.; Li, J.; More, K. L.; Dudney, N. J.; Chi, M. Interfacial Stability of Li Metal-Solid Electrolyte Elucidated via in Situ Electron Microscopy. *Nano Lett.* **2016**, *16* (11), 7030−7036.

(59) Sharafi, A.; Kazyak, E.; Davis, A. L.; Yu, S. H.; Thompson, T.; Siegel, D. J.; Dasgupta, N. P.; Sakamoto, J. Surface Chemistry Mechanism of Ultra-Low Interfacial Resistance in the Solid-State Electrolyte Li7La3Zr2O12. *Chem. Mater.* **2017**, *29* (18), 7961−7968.

(60) Steinborn, C.; Herrmann, M.; Keitel, U.; Schönecker, A.; Räthel, J.; Rafaja, D.; Eichler, J. Correlation between microstructure and electrical resistivity of hexagonal boron nitride ceramics. *J. Eur. Ceram. Soc.* **2013**, *33* (6), 1225−1235.

(61) Tian, H. K.; Xu, B.; Qi, Y. Computational study of lithium nucleation tendency in Li7La3Zr2O12 (LLZO) and rational design of interlayer materials to prevent lithium dendrites. *J. Power Sources* **2018**, *392*, 79−86.

(62) Xu, H.; Li, Y.; Zhou, A.; Wu, N.; Xin, S.; Li, Z.; Goodenough, J. B. Li3N-modified garnet electrolyte for all-solid-state lithium metal batteries operated at 40 C. *Nano Lett.* **2018**, *18* (11), 7414−7418.

(63) Wang, C.; Gong, Y.; Liu, B.; Fu, K.; Yao, Y.; Hitz, E.; Li, Y.; Dai, J.; Xu, S.; Luo, W.; et al. Conformal, nanoscale ZnO surface modification of garnet-based solid-state electrolyte for lithium metal anodes. *Nano Lett.* **2017**, *17* (1), 565−571.

(64) Fu, K.; Gong, Y.; Fu, Z.; Xie, H.; Yao, Y.; Liu, B.; Carter, M.; Wachsman, E.; Hu, L. Transient behavior of the metal interface in lithium metal−garnet batteries. *Angew. Chem., Int. Ed.* **2017**, *56* (47), 14942−14947.

(65) Riphaus, N.; Stiaszny, B.; Beyer, H.; Indris, S.; Gasteiger, H. A.; Sedlmaier, S. J. Understanding Chemical Stability Issues between Different Solid Electrolytes in All-Solid-State Batteries. *J. Electrochem. Soc.* **2019**, *166* (6), A975−A983.

(66) Zhu, Y.; He, X.; Mo, Y. Strategies based on nitride materials chemistry to stabilize Li metal anode. *Adv. Sci.* **2017**, *4* (8), 1600517.

(67) Mahankali, K.; Thangavel, N. K.; Arava, L. M. R. In Situ Electrochemical Mapping of Lithium-Sulfur Battery Interfaces Using AFM-SECM. *Nano Lett.* **2019**, *19* (8), 5229−5236.

(68) Yu, S.; Park, H.; Siegel, D. J. Thermodynamic Assessment of Coating Materials for Solid-State Li, Na, and K Batteries. *ACS Appl. Mater. Interfaces* **2019**, *11* (40), 36607−36615.

(69) Park, K.; Yu, B.-C.; Jung, J.-W.; Li, Y.; Zhou, W.; Gao, H.; Son, S.; Goodenough, J. B. Electrochemical nature of the cathode interface for a solid-state lithium-ion battery: interface between LiCoO2 and garnet-Li7La3Zr2O12. *Chem. Mater.* **2016**, *28* (21), 8051−8059.